Spatial and temporal coherence of filtered thermal light

L. Basano [a], P. Ottonello [a,b], G. Rottigni [b], and M. Vicari [a,b]

[a] *Dipartimento di Fisica – Università degli Studi di Genova,*

[b] *Istituto Nazionale di Fisica Nucleare – Sezione di Genova,*

Via Dodecaneso 33, 16146 Genova, Italy

Abstract

When a filter is placed in front of a double-slit illuminated by a primary source of finite extent, the theory of partial coherence predicts that, in general, the interference fringes will not acquire unit visibility even as the passband of the filter is made arbitrarily narrow. The effect of reducing the filter bandwidth is that the visibility of the fringes tends to the modulus of the spectral degree of coherence and that more interference fringes become visible. A systematic experimental verification of these theoretical predictions was lacking so far and is provided here thanks to the use of a highly sensitive CCD (Charge Coupled Device) camera.

OCIS codes: 030.0030, 030.1640, 040.1520

1. Introduction

After a long infancy during which optical coherence was essentially evaluated in terms of a binary variable (presence or absence of interference fringes), the theory of coherence gained a new impetus thanks to the works of van Cittert, Zernike, Wolf, Mandel and a few other researchers; in the new scenario, the center of the stage was taken by the statistical correlations between the field variables, measured at two or more space-time points.

For several decades, only the *space-time (or complex) degree of coherence*, that characterises field correlations in the space-time domain, was used to measure the partial coherence of light[1–4]. It was subsequently recognised that analysing coherence problems solely in terms of space-time correlation functions might be often inappropriate; to this end, a rigorous theory of partial coherence in the space-frequency domain was developed by Wolf[5,6]. The *spectral degree of coherence* then emerged in a natural way to characterise correlations in the space-frequency domain and began to play an important role for the study of optical phenomena. For example, the clarification of the concept of spectral purity and the topic of correlation-induced spectral changes[7] (sometimes referred to as the Wolf effect) are among the fruitful consequences of a space-frequency approach to coherence that stimulated considerable research activity.

The relevance of the degree of spectral coherence for the present work stems from an article in which Wolf[8] studied how an interference pattern is modified by placing a narrow-band filter in front of a pair of Young slits. More specifically, Wolf predicted that the maximum visibility of the fringes cannot exceed the value of the *degree of spectral coherence* of the light and the only significant effect of narrowing the filter bandwidth is that more fringes become visible.

The issue of the fringe visibility when thermal light is passed through sharply tuned filters

was also later mentioned by James and Wolf[9]. Finally, Friberg and Wolf[10] reconsidered the same problem in a different and more complete manner and confirmed the theoretical conclusions previously published by Wolf.

It is perhaps surprising that, despite their great conceptual and pedagogical importance, Wolf's predictions quoted above have not been subjected to a *systematic and quantitative experimental confirmation*; the reason of this omission is probably due to the difficulty of working with the low intensities typical of severely filtered thermal light. This work is devoted to the verification of these predictions and belongs to a line of experimental research[11,12] in which highly sensitive (possibly intensified) CCD cameras are used to quickly record and process two dimensional images.

The article is structured as follows. Sect. 2 is devoted to a short theoretical summary of the problem, whereas the description of the experiment is given in Sect. 3. The results obtained and their comparison with theory are illustrated in Sect. 4. Further comments and conclusions are presented in Sect. 5. Finally, an Appendix describes how the theoretical curves used to fit the experimental data are numerically calculated starting from a statistical model of the source.

2. Theoretical background

Let $V(P_1,t)$ and $V(P_2,t)$ be the analytic signal representations of a fluctuating light field at two points P_1 and P_2 at time t. The mutual coherence function $\Gamma_{12}(\tau)$ is defined as the cross-correlation of the field at two space time points:

$$\Gamma_{12}(\tau) = \langle V^*(P_1,t)\, V(P_2,t+\tau)\rangle. \tag{1}$$

P_j indicates the position of the j^{th} point in the field; as usual, the angle brackets denote ensemble or time average (the field is assumed to be stationary and ergodic) and the asterisk represents the complex conjugate. As regards the terminology and the notation adopted here, we make reference to the already quoted texts and review articles[1–4]. The complex degree of coherence $\gamma_{12}(\tau)$ of the light is then defined as a normalized form of the mutual coherence function:

$$\gamma_{12}(\tau) = \frac{\Gamma_{12}(\tau)}{\sqrt{\Gamma_{11}(0)\Gamma_{22}(0)}}. \tag{2}$$

The evaluation of the coherence of light in the space-frequency domain[5,6] is based on the *degree of spectral coherence* $\mu_{12}(\omega)$ that is defined as follows:

$$\mu_{12}(\omega) = \frac{W_{12}(\omega)}{\sqrt{W_{11}(\omega)W_{22}(\omega)}}, \tag{3}$$

where $W_{jk}(\omega)$ is the Fourier Transform of $\Gamma_{jk}(\tau)$, $(j, k = 1, 2)$:

$$W_{jk}(\omega) = \int \exp(-i\omega\tau)\, \Gamma_{jk}(\tau)\, \mathrm{d}\tau. \tag{4}$$

The analysis of the correct relationship between $\gamma_{12}(\tau)$ and $\mu_{12}(\omega)$ was explicitly performed by Friberg and Wolf[10].

Let's consider the interference pattern produced when thermal light, emitted by an extended source, goes through a pair of Young slits in front of which a narrow-band filter,

centered at ω_0, is placed (Fig. 1). It has been shown[8,10] that:

$$\gamma_{12}^{+}(0) = \mu_{12}(\omega_0), \tag{5}$$

i.e. the equal-time complex degree of coherence of the *filtered light*, $\gamma_{12}^{+}(0)$, is equal to the degree of spectral coherence $\mu_{12}(\omega_0)$. In turn, as is well known, the modulus of $\mu_{12}(\omega_0)$ is equal to the fringe visibility at the center of the interference pattern. Hence "*the maximum visibility of the interference fringes formed by the filtered light will not, in general, tend to unity as the passband of the filter decreases*"[8,13]. The only effect of filtering is that more fringes become visible; in more intuitive words, temporal coherence is affected by filtering while spatial coherence is not.

3. Description of the experiment

A. Instrumentation

The experimental setup (Fig. 1) is implemented to allow a systematic verification of Eq. (5) and some of its consequences.

In the first place it includes the primary extended source, consisting of a halogen lamp located in front of a single slit. The light exiting the primary aperture then goes through the Young double-slit and is eventually recorded by a CCD camera (Thomson TH79KA96) located some distance away on the optical axis. Filters of various bandwidths centered around two fixed wavelengths (see Tab. 1) are successively positioned in front of the double-slit. In order to minimize the optical complexity of the system and the risk of spurious effects we chose not to use any lens. Renouncing to Fraunhofer diffraction, however, did not make the theoretical predictions more difficult; actually it simplified them because, as

we describe in the Appendix, the shapes of the theoretical fringes are obtained by means of numerical simulations based on Matlab programming.

The geometrical parameters of our experimental setup (Fig. 1) are the following (all values are in meters and the relative error is of the order of 10^{-2}): width of primary slit (SS): $a = 1.35 \cdot 10^{-4}$; width of each double-slit (DS): $b = 1.22 \cdot 10^{-4}$; distance between double-slit centers: $d = 6.25 \cdot 10^{-4}$; distance between primary source and double-slit: $r = 0.312$; distance between double-slit and image plane: $R = 0.601$.

B. Data acquisition and processing

The axis of the camera is first oriented so that the CCD pixel columns are aligned with the direction of the fringes, after which the image of the fringe patterns (Fig. 2a) is directly stored as a 2-D record by means of a Genesis data acquisition board (Matrox, Dorval, Quebec, Canada). By summing the values recorded in each column, the 2-D fringe system is then converted into a 1-D intensity profile that may be thus regarded as an ensemble-average exhibiting a highly enhanced signal-to-noise ratio.

The typical profile that emerges at this point is curve A of Fig. 2b. Even a cursory inspection of this graph reveals that significant processing of the data is still needed to obtain an acceptable result; as we describe below, this is due to some disturbances related to the constructional details of the camera.

We first note that the sought-after double-slit interference fringes (located in the right part of the graph) appear to be superimposed on a system of rather regular ripples; the latter ones are generated by the inner periodic spatial structure of a fiber taper glued to the CCD surface. The box-shaped taper (T in Fig. 1) consists of a square array containing approximately 3000×3000 fibers; the taper is glued (by the manufacturer) to the 1024×1024-pixel CCD surface for the purpose of coupling the latter, in case of necessity, to an image

intensifier. In order to reduce cross-talk between adjacent bunches, these are separated from one another by a layer of Extra Mural Adsorber (EMA). It is this regular array of optically isolated bunches that generates the periodic structure of the ripples.

However, if this were the only spurious effect related to the constructional details of the camera, the double-slit fringes should appear superimposed on a *horizontal* sequence of ripples; what we actually observe (curve B in Fig. 2b), instead, is that the ripple system is, in turn, superimposed on a lower spatial-frequency modulation. The latter is due to a fabrication inaccuracy: the geometrical and optical features of the glue layer that couples the taper to the CCD surface are not strictly homogeneous and generate a modulation in the transmitted light. This also explains why the double-slit fringes appear to be considerably displaced to the right in figures 2a and 2b: we intentionally selected the camera position so as to let the fringes fall in the flattest region of the transmitted light modulation.

Finally, unavoidable lacks of homogeneity of individual fibers and pixel sensitivity represent a further source of (higher spatial-frequency) noise: this is revealed by the jagged appearance of the ripples. The combination of all these factors produces the curve of the overall systematic noise that affects the signal to be analyzed (graph B in Fig. 2b). Only to improve the visualization of the total systematic error, graph B in Fig. 2b has been shifted downwards by an amount sufficient to avoid any overlapping with graph A.

The disturbance described so far, however, is strictly deterministic and can be efficiently subtracted out by means of a preliminary calibration; in this connection, let's note how closely both the long term modulation and the small scale jitters in graphs A and B visually match. The end result of the image processing is shown by graph C, that is obtained by subtracting B from A and is the typical representative of the intensity profiles patterns we used to obtain the values of the degree of coherence reported in the next Section.

Perhaps it is worth pointing out one more fact relating to the calibration procedure. Usually, in optical measurements, stray light is a negative factor which one always attempts to minimize. In our case the largely dominant error is of systematic origin and some level of stray light turns out to play a useful role; in fact we exploited it to accurately monitor the distortions produced by instrumental features or imperfections and to get a virtually complete nulling of deterministic errors. This was achieved by preliminarily blanking only the double-slit apertures to obtain, before each run, the graph of the systematic noise (B).

4. Results

We consider separately the measurements through which Eq. (5) is verified and those related to the enhancement of temporal coherence by means of filtering.

A. As the width of the filter decreases, the visibility of the fringes, by Eq. (5), tends to the modulus of the spectral degree of coherence

We tested this prediction by performing a sequence of measurements in two different optical bands centered, respectively, at wavelengths $\lambda_1 = 488$ nm and $\lambda_2 = 633$ nm (these choices were suggested by the wide availability of commercial filters at these wavelengths). The bandwidths of the filters used are listed in Tab. 1.

Furthermore, an additional run was carried out using the full spectral width of the halogen lamp (approximately 200 nm). The results (reproduced in Fig. 3) clearly show that, within the experimental errors, *no significant variation of the degree of coherence takes place*. As filters of narrower and narrower bandwidths are employed, the visibility, for both wavelengths, approaches values which are definitely smaller than 1.

Moreover, these extrapolated values agree fairly well with the moduli of the degree of spectral coherence, 0.70 at 633 nm and 0.53 at 488 nm, that we obtained by running

the numerical simulation program using a bandwidth of 1 nm. These values are slightly smaller than those usually predicted, for the ideal case of infinitely thin slits and Fraunhofer diffraction, according to the relation:

$$\mu = \frac{\sin(x)}{x}, \qquad \text{where} \qquad x = \frac{\pi a d}{\lambda r}. \tag{6}$$

In fact, by inserting the numerical values reported at the end of Sec. 4 A into Eq. (6), we obtain the results 0.72 and 0.56.

B. As the bandwidth of the filter decreases, more fringes become visible

It is equally simple to verify that, unlike spatial coherence, temporal coherence is significantly enhanced by progressively reducing the filter's width. The most noticeable visual change associated with the improvement of temporal coherence is that more fringes take shape and become visible as the frequency spread of the light is decreased.

This behavior is clearly illustrated by the experimental graphs reported in Fig. 4. From Fig. 4a (unfiltered lamp) we can see that only two fringes are visible on each side of the central maximum; but when very narrow filtering is applied (1 nm, Fig. 4d) at least five fringes are clearly discernible in the same zone of the image. *Note, however, that the maximum contrast has not appreciably changed from frame a) to d), despite the filter's width having decreased by more than two orders of magnitude.*

5. Comments and conclusions

In this Section we discuss a few points that, in our opinion, can usefully complement the description of the experiment given above.

1. The visibility of the fringes produced by the *unfiltered* lamp (marked as an open circle

in the upper right of Fig. 3), *is much closer to the 633 nm sequence than to the 488 nm sequence*. This is understandable because the lamp emits more intensively at longer than at shorter wavelengths and the spectral response of the camera is also significantly biased towards the red end of the visible spectrum. As a result, the fringe system for the unfiltered lamp (Fig. 4a) and the one for the 130 nm-wide filter centred at 633 nm (Fig. 4b) turn out to be very similar.

2. Also the plots in Fig. 4c (10 nm bandwidth filter) and Fig. 4d (1 nm bandwidth filter) strongly resemble one another, but for quite a different reason. In the visible range, a spectral width of 10 nm corresponds to a relative "uncertainty" in wavelength of about 2%; as a consequence, this is the order of magnitude of the spatial blurring of the fringes caused by the incoherent superposition of the different wavelengths composing the light. It thus follows that the fringes produced by visible light of the same central wavelength, but with spectral widths differing by less than 10 nm, are practically indistinguishable.

3. An important consequence of the previous reasoning is that, to an accuracy considerably better than 1%, the results achieved for the filter band-pass of 1 nm can be automatically extended downward to light of *arbitrarily narrow* spectral width (and this was indeed the main target of our work).

4. On the basis of the two sets of experimental points in Fig. 3, one might be led to conjecture that the visibility at a given central wavelength does not depend on the filter bandwidth (we owe this remark to the constructive criticism of a Reviewer). To this end, it is perhaps worth noticing that, in practice, this "constancy" takes place only over an interval of limited extent (in our case, from 1 nm to 80 nm for the 488 nm

sequence and from 1 nm to 130 nm for the 633 nm sequence); this constancy should not be unduly extrapolated to larger intervals. The last statement can be intuitively explained as follows: by progressively widening the bandwidth of a filter centered at any preset frequency, one must eventually reach a point where the filter is so wide that the lamp is not filtered at all. At this point, the measured visibility must be equal to that of the unfiltered lamp, which may be significantly different from the value it assumed when the filter bandwidth was very narrow. This reasoning militates against the constancy of visibility over too large bandwidth intervals. At low bandwidths, instead, the visibility remains fairly independent of the bandwidth for the reasons described in item 2 above.

5. In the early stage of the experiment the CCD camera was equipped with an intensifier in order to work with brighter images. However, when we began to compare experimental results with theoretical predictions we had to face a significant discrepancy which we were at first unable to link to any reasonable source of error. More precisely, the optical visibility recorded by the camera proved to be systematically smaller than the theoretically expected one; in addition, the measured visibility turned out to be very small when the fringes were very close to one another. At this point we began a systematic investigation on this effect and, after a few trials, we came to the conclusion that, when the image to be analyzed consists of narrow vertical stripes (as is approximately the case with the measurement of optical visibility in a fringe system), the use of an intensifier leads to the generation of significant distortion. This emerged clearly when identical images were analyzed with and without intensifier; of course we also ascertained that the effect was not due to a malfunctioning of the intensifier used.

We do not enter the details of this behavior because we subsequently decided to continue our experiment without making recourse to an intensifier and using instead a primary lamp of enhanced power; this solution proved to be sufficient for our goal. In our opinion, however, the intensifier-generated distortion problem deserves consideration whenever the optical visibility of very weak details is to be measured and is presently the subject of an experiment under way.

Appendix: Numerical calculations of theoretically expected curves

Our confidence in the reliability of the results that we were progressively gathering during our work was favorably conditioned by the possibility of comparing them, at any moment, with theoretical expectations. This was obtained by simulating the real experimental process through a Matlab program. To this end, for each wavelength selected in the range of interest, the primary aperture is modeled as an array of statistically independent radiators; the phase and the amplitude are attributed to each emitter according to a random choice; by this procedure, a random complex electric vector E_p is built at each point of the primary aperture.

Two propagation matrices, $M_{PS,R}$ (for the right slit) and $M_{PS,L}$ (for the left slit) are then defined whose elements represent the exponentiated phase delay from the generic point P in the primary aperture to a generic point S in the double-slit apertures. The matricial product $E_p \cdot M_{PS,R}$ then allows to find the complex electric vector $E_{S,R}$ in the right slit (with a similar computation for points in the left slit). Using an entirely analogous procedure (and notation), a pair of matrices $M_{SI,R}$ and $M_{SI,L}$ allow to compute the complex electric vectors $E_{I,R}$ and $E_{I,L}$ generated in the image plane respectively by the right and the left slit; by superposing these two electric vectors, and by taking the square of the modulus of the sum, one obtains the light intensity at each point of the image plane I. At this point, however,

the simulation program is not yet complete because the result we have obtained gives the intensity produced in the image plane by a *particular instantaneous* attribution of random phases and amplitudes to each one of the emitters located in the primary aperture. It is still necessary to simulate the existence of a *finite integration time*, over which the phases and the amplitudes are allowed to randomly change, while the intensity is continuously being accumulated in the image plane. This is obtained by proceeding to a new random attribution of phases and amplitudes, adding the newly computed intensity to the previous intensity and iterating the process as many times as necessary. The number of iterations required to obtain acceptably stable results has turned out to be of the order of 10^3.

The lower frame in Fig. 5 reproduces the result of an experimental run performed using a 1 nm bandwidth filter at 633 nm, while the upper frame depicts the graph we obtained by numerically simulating the same conditions.

The reason why just the pair of curves in Fig. 5 are proposed is not because their agreement is particularly good; using the CCD technique and the image processing described above, the level of matching between experiment and theory shown in Fig. 5 is representative of all runs.

As a final comment it is worth recalling that, for the problem discussed in this paper, numerical simulations allow to cope very naturally with some potentially disturbing elements: the finite (and possibly unequal) widths of the double-slits, an inhomogeneous distribution of brightness on the primary slit, an axial asymmetry of the optical arrangement or the fact that Fraunhofer diffraction is not employed; all these elements, taken together, might render an accurate *analytical solution* rather difficult to obtain. For readers interested in the above simulation, a Matlab program is available on request.

Acknowledgements

We are deeply indebted to Professor Emil Wolf for drawing our attention to the problem tackled in this work, for encouraging the research presented here and for offering us many precious suggestions of which we have benefited during the preparation of the manuscript.

References

1. M. Born, E. Wolf, *Principles of optics* (Cambridge University Press, Cambridge, 1999), 588.
2. M. J. Beran, G. B. Parrent, Jr., *Theory of partial coherence* (Prentice Hall, Englewood Cliffs, N. J., 1964).
3. L. Mandel, E. Wolf, "Coherence properties of optical fields", Rev. Mod. Phys. **37**, 231–287 (1965).
4. L. Mandel and E. Wolf, *Optical Coherence and Quantum Optics* (Cambridge University Press, Cambridge, 1995), 307–318.
5. E. Wolf, "New theory of partial coherence in the space-frequency domain. Part I: Spectra and cross spectra of steady state sources", J. Opt. Soc. Am. A **72**, 343–351 (1982).
6. E. Wolf, "New theory of partial coherence in the space-frequency domain. Part II: Steady-state fields and higher-order correlations", J. Opt. Soc. Am. A **3**, 76–85 (1986).
7. E. Wolf, D. F. V. James, "Correlation-induced spectral changes", Rep. Prog. Phys. **59**, 771–818 (1996).
8. E. Wolf, "Young's interference fringes with narrow-band light", Opt. Lett. **8**, 250–252 (1983).
9. D. F. V. James, E. Wolf, "Some new aspects of Young's interference experiment", Phys. Lett. A **157**, 6–10 (1991).

10. A. T. Friberg, E. Wolf, "Relationships between the complex degrees of coherence in the space-time and in the space-frequency domains", Opt. Lett. **20**, 623–625 (1995).

11. L. Basano, S. Leporatti, P. Ottonello, V. Palestini, R. Rolandi, "Measurements of surface roughness: use of a CCD camera to correlate doubly scattered speckle patterns", Appl. Opt. **34**, 7286–7290 (1995).

12. L. Basano, P. Ottonello, G. Rottigni, M. Vicari, "Degree of spectral coherence, space-frequency plots and correlation-induced spectral changes", Opt. Commun. **207**, 77–83 (2002).

13. Ref. 4, pp. 174–176.

List of Figure Captions

Fig. 1. Experimental setup: L = halogen lamp; SS = primary slit; DS = double-slit; F = filter; T = fiber taper glued to the CCD surface (see text).

Fig. 2. a) Image of the fringe pattern detected by the CCD camera (at 633 nm wavelength and 1 nm bandwidth). b) Graph A: Intensity profile obtained from Fig. 2a – Graph B: Overall systematic error (shifted downwards to avoid overlapping with graph A) – Graph C: Intensity profile after correction of systematic error. In graphs A, B, C vertical scales are in arbitrary units.

Fig. 3. Experimental measurement of fringe visibility vs Log10 of bandwidth (nm) for two sequences of filters centered at wavelengths 633 nm (circles) and 488 nm (squares). The open circle marks the result for the unfiltered lamp. The points of each sequence are joined by dotted lines only for clarity of visualization.

Fig. 4. Normalized experimental records of interference fringes. a) unfiltered lamp; b) 130 nm bandwidth; c) 10 nm bandwidth; d) 1 nm bandwidth. Plots b), c), d) are for a central wavelength of 633 nm.

Fig. 5. a) Numerical simulation for 1 nm-passband centered on the wavelength of 633 nm. b) Experimental results for the same conditions used in the simulation – In both graphs the vertical scale refers to normalized values.

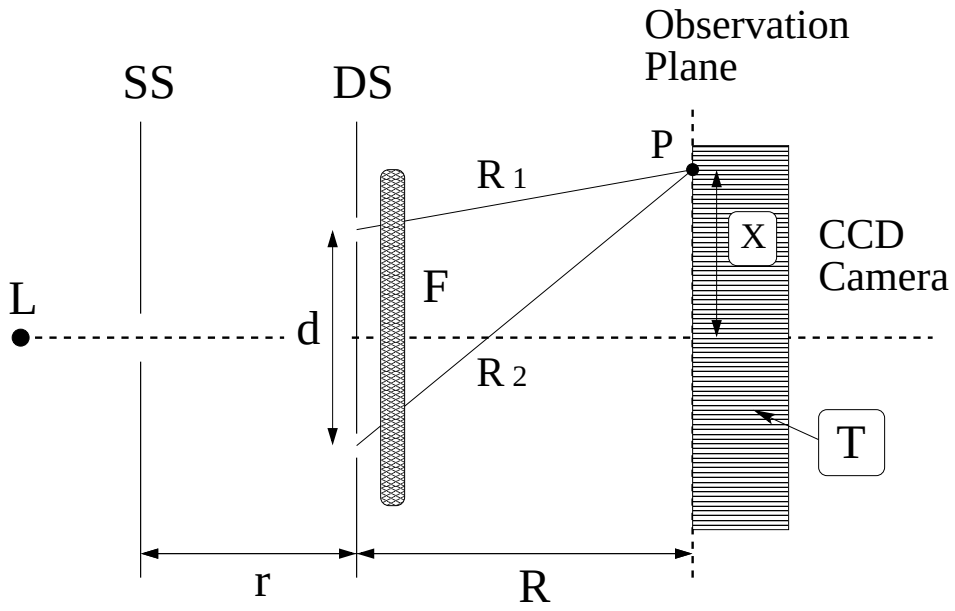

Fig. 1. Experimental setup: L = halogen lamp; SS = primary slit; DS = double-slit; F = filter; T = fiber taper glued to the CCD surface (see text).

basfig1.eps.

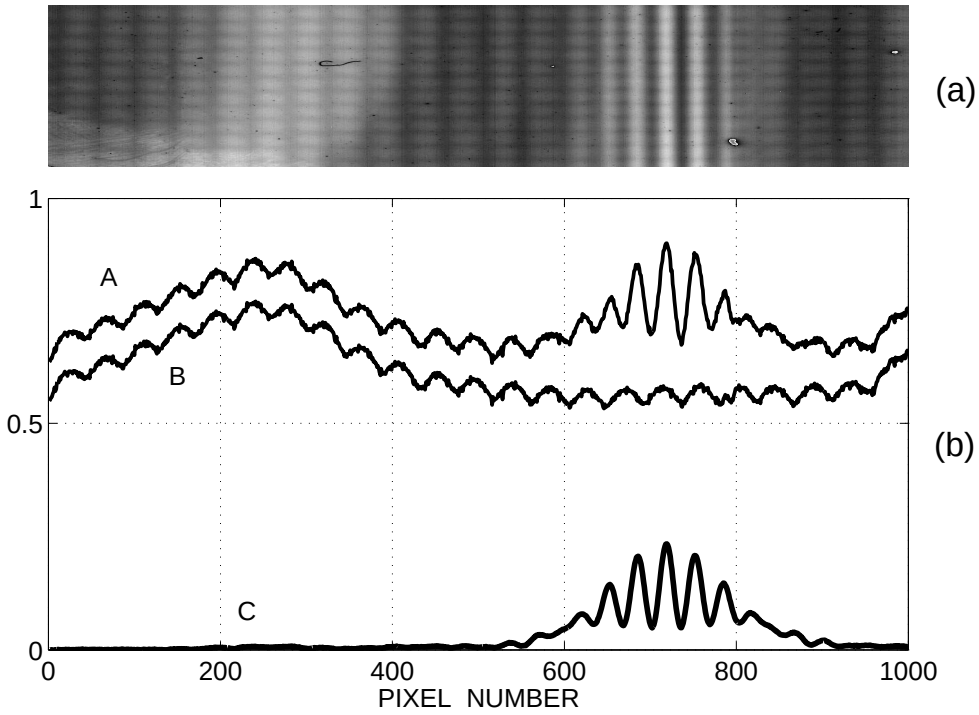

Fig. 2. a) Image of the fringe pattern detected by the CCD camera (at 633 nm wavelength and 1 nm bandwidth). b) Graph A: Intensity profile obtained from Fig. 2a – Graph B: Overall systematic error (shifted downwards to avoid overlapping with graph A) – Graph C: Intensity profile after correction of systematic error. In graphs A, B, C vertical scales are in arbitrary units.

basfig2.eps.

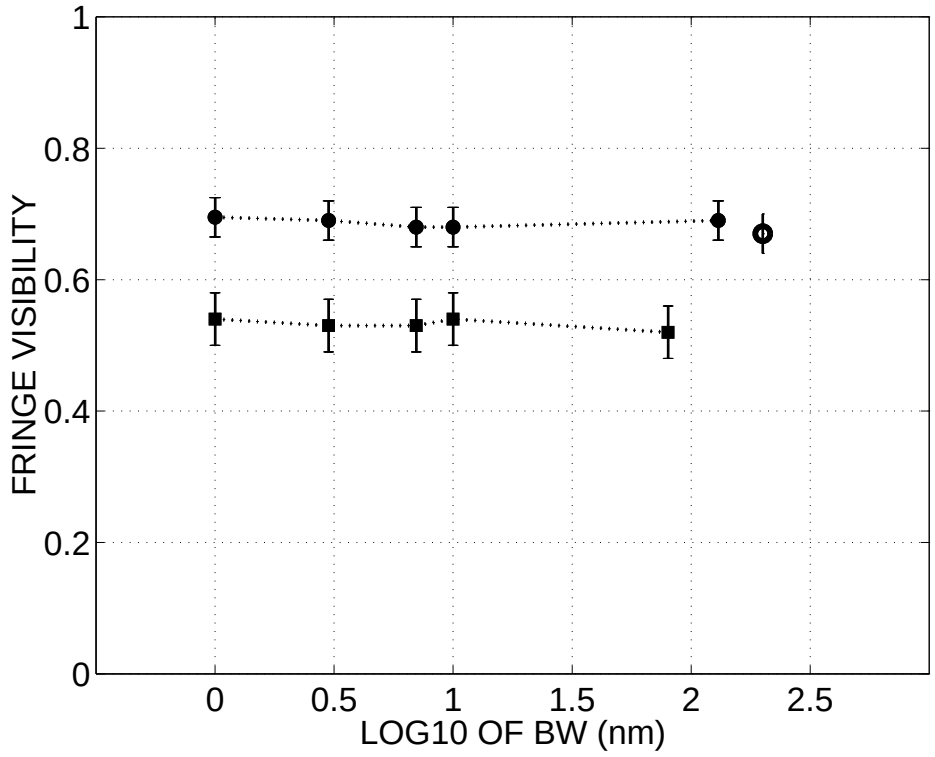

Fig. 3. Experimental measurement of fringe visibility vs Log10 of bandwidth (nm) for two sequences of filters centered at wavelengths 633 nm (circles) and 488 nm (squares). The open circle marks the result for the unfiltered lamp. The points of each sequence are joined by dotted lines only for clarity of visualization.

basfig3.eps.

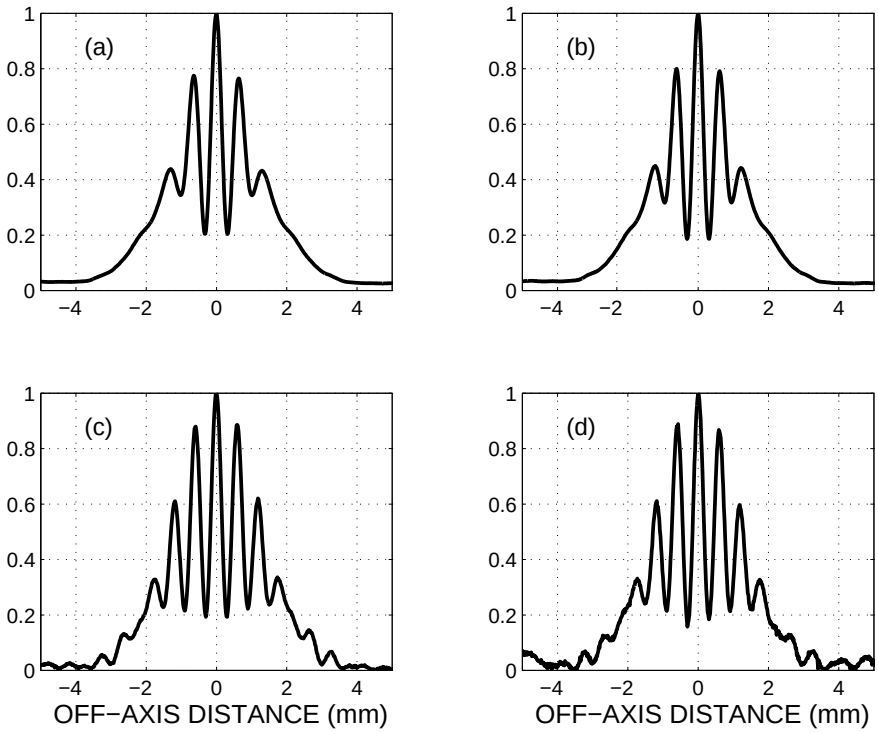

Fig. 4. Normalized experimental records of interference fringes. a) unfiltered lamp; b) 130 nm bandwidth; c) 10 nm bandwidth; d) 1 nm bandwidth. Plots b), c), d) are for a central wavelength of 633 nm.

basfig4.eps.

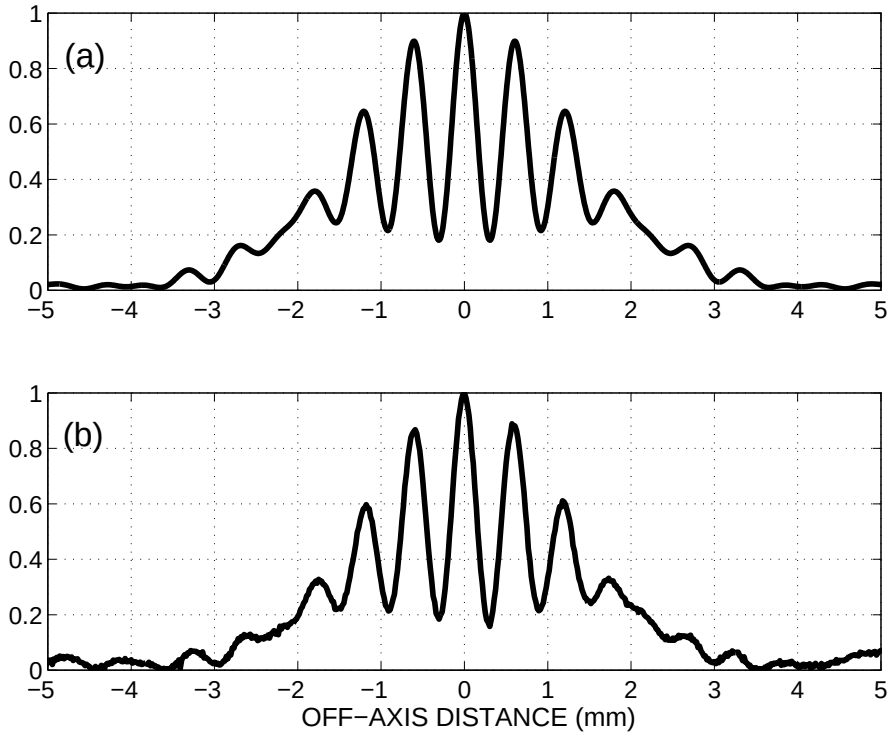

Fig. 5. a) Numerical simulation for 1 nm-passband centered on the wavelength of 633 nm. b) Experimental results for the same conditions used in the simulation – In both graphs the vertical scale refers to normalized values.

basfig5.eps.

Table 1. Filters employed in the experiment

Central Wavelength (nm)	Bandwidth (nm)				
633	1	3	7	10	130
488	1	3	7	10	80